Case C1.3: Flow Over the NACA 0012 Airfoil: Subsonic Inviscid, Transonic Inviscid, and Subsonic Laminar Flows

Masayuki Yano* and David L. Darmofal†

Aerospace Computational Design Laboratory, Massachusetts Institute of Technology

I. Code Description

ProjectX is a high-order, adaptive discontinuous Galerkin finite element solver. The DG discretization uses Roe's approximate Riemann solver[1] for the inviscid numerical flux and Bassi and Rebay's second discretization (BR2)[2] for the viscous numerical flux. In the presence of shocks, artificial viscosity is added in a smooth manner using a jump-based discontinuity sensor and the shock PDE introduced by Barter and Darmofal[3] with a few additional modifications.[4] The solution to the discretized system is obtained using a Newton-based nonlinear solver with pseudo-time continuation. The linear system arising in each pseudo-time step is solved using GMRES,[5] preconditioned with an in-place block-ILU(0) factorization[6] with minimum discarded fill reordering and $p = 0$ algebraic coarse correction.[7]

An output-based, anisotropic simplex adaptation algorithm is used to control the discretization error.[8] The algorithm iterates toward a mesh that minimizes the output error for a given number of degrees of freedom. The anisotropic adaptation decisions are entirely driven by the behavior of an output-based *a posteriori* error estimate; thus, the method handles any discretization order, naturally incorporates both the primal and adjoint solution behaviors, and robustly treats irregular features. The output error estimate uses the dual-weighted residual (DWR) method of Becker and Rannacher.[9] A new mesh that conforms to the metric request is generated using using BAMG (Bidimensional Anisotropic Mesh Generator),[10] and higher-order, globally curved meshes are constructed through linear elasticity.[11]

II. Case Description

II.A. Flow Conditions

Case C1.3 considers three separate flows over a NACA 0012 airfoil:

1. Subsonic, inviscid flow with $M_\infty = 0.5$, $\alpha = 2^\circ$
2. Transonic, inviscid flow with $M_\infty = 0.8$, $\alpha = 1.25^\circ$
3. Subsonic, laminar flow with $M_\infty = 0.5$, $\alpha = 1^\circ$, $Re_c = 5,000$, $Pr = 0.72$ (adiabatic wall)

For each flow condition, we specify the appropriate total temperature, the total pressure, and the flow angle at the inflow and the static pressure at the outflow.

II.B. Domain Specification

The (modified) NACA 0012 airfoil is defined by

$$y = \pm 0.6(0.2969\sqrt{x} - 0.1260x - 0.3516x^2 + 0.2843x^3 - 0.1036x^4).$$

*Doctoral candidate, AIAA student member, 77 Massachusetts Ave. 37-442, Cambridge, MA, 02139, myano@mit.edu
†Professor, AIAA associate fellow, 77 Massachusetts Ave. 37-451, Cambridge, MA, 02139, darmofal@mit.edu

In order to determine an appropriate farfield boundary location that results in the drag sensitivity of less than 10^{-6}, a square outer domain boundary is parametrized by the half-edge length, R (i.e. the square is $2R \times 2R$). The farfield locations of

$$R \in \{50c, 200c, 800c, 3200c, 10000c, 40000c\}$$

are considered for the parametric study. Figure 1 shows the sensitivity of the drag coefficient to the farfield location for the subsonic inviscid and subsonic laminar flow conditions. Each solution is obtained using the adaptive $p = 3$, dof $= 40000$ discretization, which results in the c_d error of approximately 3×10^{-8}; thus each solution is grid converged (for the purpose of the sensitivity study), and the c_d variation is essentially due to the difference in the farfield location. To capture the leading error due to the vortex singularity (and the source singularity for the laminar case), we have fit the c_d against $1/R$. The result suggests that $R = 10^4 c$ is sufficient to meet the required c_d variation of less than 0.01 counts.

Note that sensitivity study is not performed for the transonic inviscid flow due to the difficulty of controlling the discretization error to less than 0.01 counts. Without the ability to drive the discretization error to less than the required farfield error level, the parametric study could not be performed. Thus, for consistency, $R = 10^4 c$ mesh is used for the transonic case.

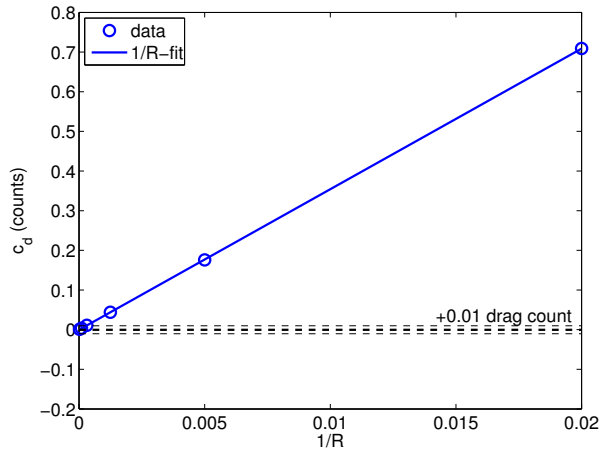

(a) subsonic inviscid c_d vs. R

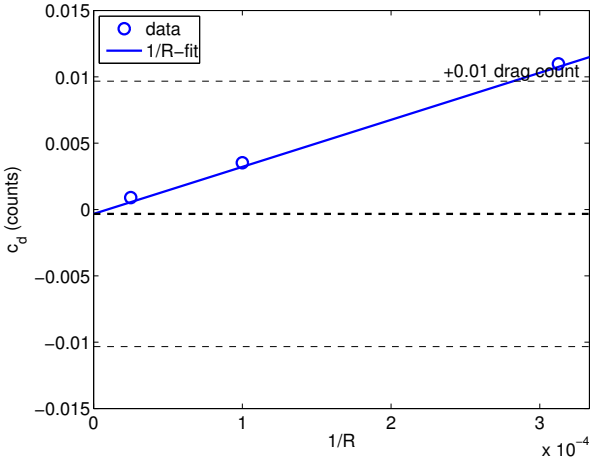

(b) subsonic inviscid c_d vs. R (zoom)

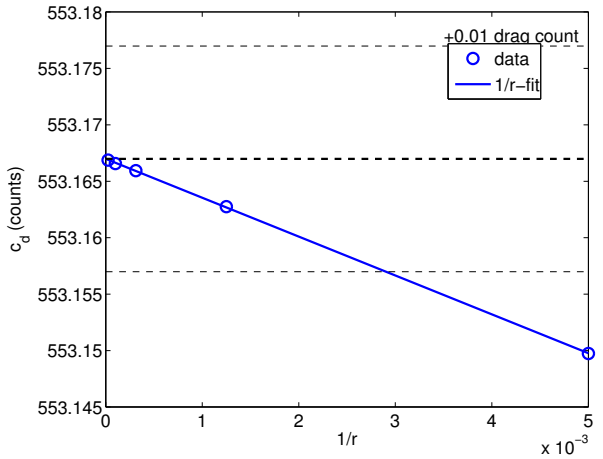

(c) subsonic laminar c_d vs. R

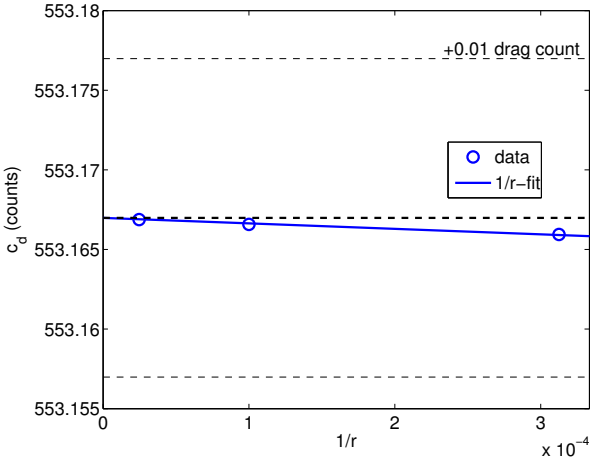

(d) subsonic laminar c_d vs. R (zoom)

Figure 1. Farfield location sensitivity for the subsonic inviscid and laminar flows.

II.C. Convergence Criterion

The ℓ^2 norm of the DG residual of non-dimensionalized Navier-Stokes equations is used to monitor convergence to the steady state. Our solver operates on non-dimensionalized variables

$$\rho^* = \frac{\rho}{\rho_\infty}, \quad u^* = \frac{u}{\|V_\infty\|}, \quad v^* = \frac{u}{\|V_\infty\|}, \quad p^* = \frac{p}{\rho_\infty \|V_\infty\|^2}, \quad e^* = \frac{e}{\|V_\infty\|^2},$$
$$R^* = \frac{R}{c_v}, \quad T^* = \frac{T}{\|V_\infty\|^2/c_v}, \quad \text{and} \quad \mu^* = \frac{\mu}{\rho_\infty L_\infty V_\infty}.$$

The DG residual is computed against the Lagrange test functions with equidistributed nodes, and the ℓ^2 norm of the residual is converged to 1×10^{-9}. (Note that the solver time would not be significantly influenced for any reasonable choice of the tolerance (say $< 1 \times 10^{-7}$), as we achieve Newton convergence in this regime. With the specified non-dimensionalization, the difference between the ℓ^2 residual and the mass residual is well within this offset.)

II.D. Hardware Specification

All computations are performed in serial on a Linux machine with an Intel i7-2600 processor and 16 Gbytes of RAM. The machine produces a Taubench time of 6.60 seconds.

II.E. Residual Timing

The time for performing a single dof $= 250,000$ residual evaluation, including the full Jacobian for the implicit solver, is summarized in Table 1. The residual evaluation for subsonic inviscid, transonic inviscid, and subsonic laminar cases are performed on meshes containing 13076, 26954, and 13844 elements, respectively, and the timings are scaled to 250,000 degrees of freedom. The laminar case is slower than the inviscid case due to the additional evaluation of the viscous flux. The transonic case is slower than the subsonic inviscid case due to the evaluation of the shock capturing term, which adds an extra PDE, and the viscous term arising from the addition of artificial viscosity.

	time (work unit)		
p	subsonic inviscid	transonic inviscid	subsonic laminar
1	0.64	2.61	1.11
2	0.54	2.06	0.96
3	0.66	-	1.15

Table 1. dof $= 250,000$ residual evaluation time (including the full Jacobian construction).

II.F. Initial Mesh

The initial mesh used for all three cases is shown in Figure 2. The airfoil geometry is represented using $q = 3$ simplex elements. After each mesh refinement, the geometry representation is refined by re-sampling from the analytical NACA 0012 geometry.

II.G. Adaptation Procedure and Data Reported

The ranges of the solution orders, p, and the number of degrees of freedom, dof, considered for the subsonic inviscid and subsonic laminar cases are

$$p \in \{1, 2, 3\} \quad \text{and} \quad \text{dof} \in \{2500, 5000, 10000, 20000\},$$

and those for the transonic inviscid case are

$$p \in \{1, 2\} \quad \text{and} \quad \text{dof} \in \{2500, 5000, 10000, 20000, 40000\}.$$

For each p-dof combination, a family of optimized meshes are generated using our anisotropic simplex mesh adaptation algorithm.[8] The output adapted is the drag on the airfoil for the all cases.

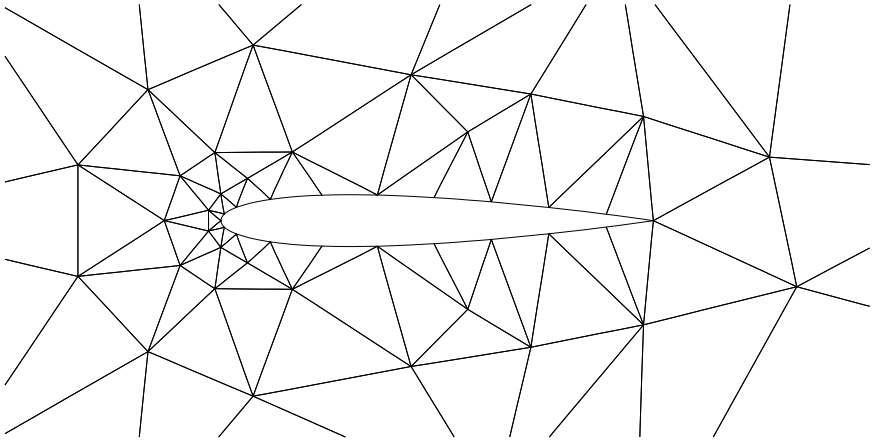

Figure 2. Initial 303-element mesh.

As in Case 1.1, the performance of each p-dof is assessed by averaging the error obtained on five realization of meshes in the family. The time reported is the total time required to reach the first realization of the p-dof-optimized mesh starting from the initial mesh shown in Figure 2; this includes multiple flow solves and adaptation overhead. (See the description provided in Case 1.1 for details.)

III. Results: Subsonic Inviscid ($M_\infty = 0.5$, $\alpha = 2^\circ$)

III.A. Error Convergence

The reference solution is obtained using the adaptive $p = 3$, dof = 80000 discretization. The reference c_d and c_l values used for this case are

$$c_d = 3.511 \times 10^{-7} \pm 3 \times 10^{-10}$$
$$c_l = 0.28653.$$

The error estimate for c_d is based on the adjoint-based error estimate and the fluctuation in the c_d value for this family of optimized meshes. We caution that the c_l reference value is likely less accurate than the drag value due to the ill-behaved lift output with the weakly enforced Kutta condition.

Figure 3(a) shows the convergence of the drag coefficient against the number of degrees of freedom. With the aggressive refinement toward the trailing edge singularity, the adaptive scheme effectively contains the effect of the singularity and recovers the optimal convergence rate of $h^{2p+1} = (\text{dof})^{-(p+1/2)}$ for the drag output. (Note that the optimal output convergence rate for an inviscid problem is h^{2p+1} for dual-consistent discretizations. The higher convergence rate observed for the $p = 3$ case is due to the dof = 10000 solution not being in the asymptotic range.) The higher-order discretizations outperform the $p = 1$ scheme in terms of c_d accuracy per degree of freedom. In fact, even for the c_d error as high as a few drag counts, the $p > 1$ discretizations are more effective than the $p = 1$ discretization. Figure 3(b) shows that the higher-order discretizations are advantageous than the $p = 1$ discretization also in terms of computational time.

Figures 3(c) and 3(d) show the convergence of (or the lack there of) the lift coefficient with mesh refinement. The lift output is not well-behaved due to the weakly enforced Kutta condition.

III.B. Comparison of Adapted Meshes

Drag-adapted meshes for this subsonic inviscid flow at select p-dof combinations are shown in Figure 4. In general, adaptation targets the singularities at the trailing and leading edges. Even though an anisotropic adaptation algorithm is employed, refinement is essentially isotropic.

Comparison of the $p = 1$, dof = $20,000$ mesh (Figure 4(a)) and the $p = 3$, dof = $5,000$ mesh (Figure 4(b)) reveals the diffeences in the meshes required to achieve the drag error level of approximately 3×10^{-5} using the $p = 1$ and $p = 3$ discretizations. The $p = 3$ mesh is significantly sparser than the $p = 1$ mesh in the

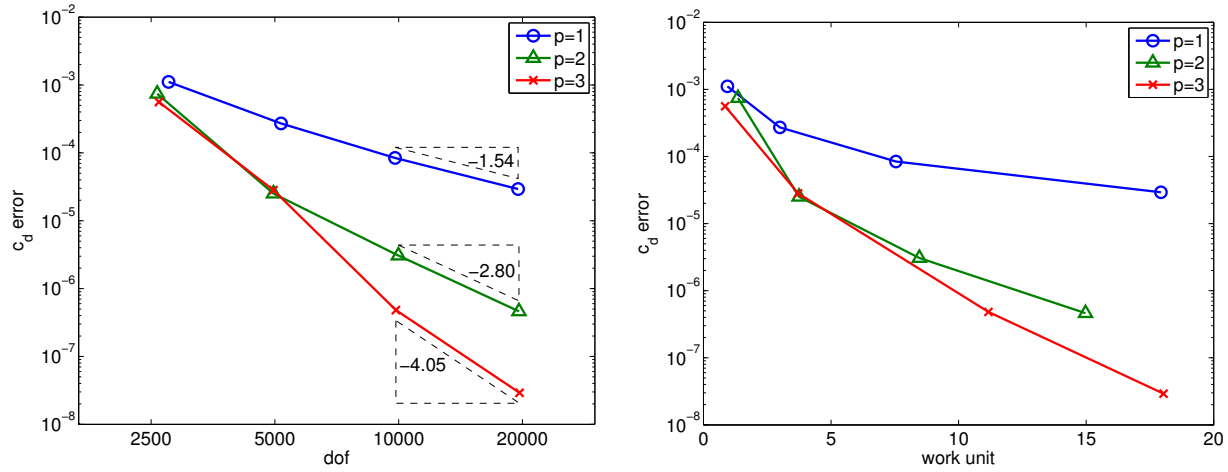

(a) c_d vs. dof (b) c_d vs. work unit

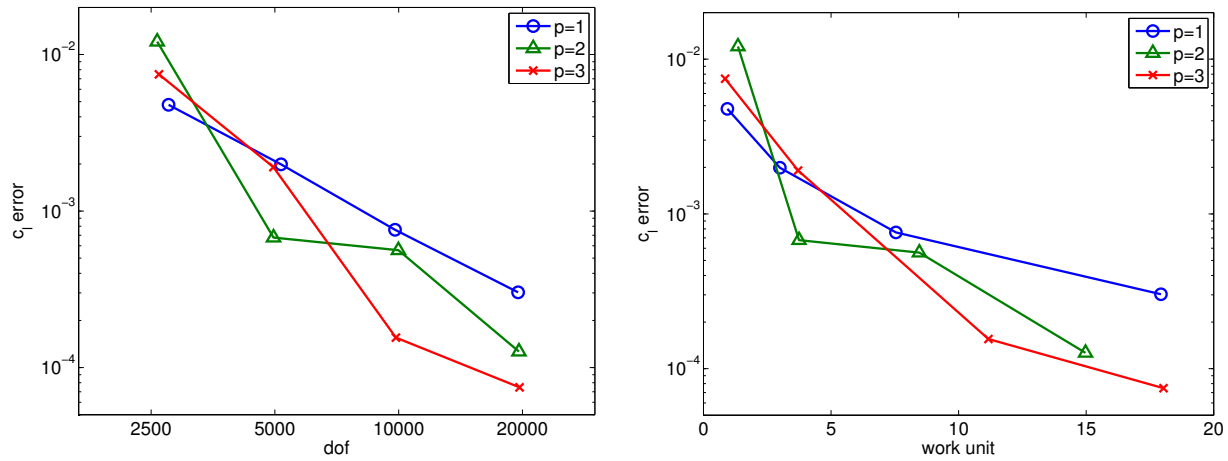

(c) c_l vs. dof (d) c_l vs. work unit

Figure 3. Error convergence for the subsonic inviscid case.

smooth region. It is worth noting that the adaptive $p = 3$ discretization achieves the drag error level of less than 0.3 counts using only 500 elements.

Comparison of the $p = 3$, dof $= 5,000$ mesh (Figure 4(b)) and the $p = 3$, dof $= 20,000$ (Figure 4(c)) mesh shows how the mesh evolves for a given p to achieve a lower error level. In increasing the number of degrees of freedom by a factor of four, the diameter of the trailing edge elements decreases from $h_{\text{te}} = 5 \times 10^{-2}$ to 2×10^{-5}, i.e. the trailing edge element diameter decreases by a factor of approximately 2500, whereas uniform refinement would have resulted in the diameter decreasing by a factor of two. The refinement is clearly not uniform. The aggressive refinement toward the trailing edge is necessary to contain the effect of the geometry-induced singularity.

III.C. Adaptive vs. Uniform Refinement

Figure 5 compares the drag error convergence results obtained using adaptive refinement and a step of uniform refinement starting from select adapted meshes. Due to the trailing edge singularity, the convergence rate of the uniform refinements are limited by the regularity of the solution. Thus, the aggressive refinement towards the trailing edge is necessary to recover the optimal convergence rate of $(\text{dof})^{-(p+\frac{1}{2})}$ (or h^{2p+1}). In particular, even if an optimal mesh distribution is obtained at a lower number of degrees of freedom, all successive refinement must be adaptive to realize the benefit of the higher-order discretization.

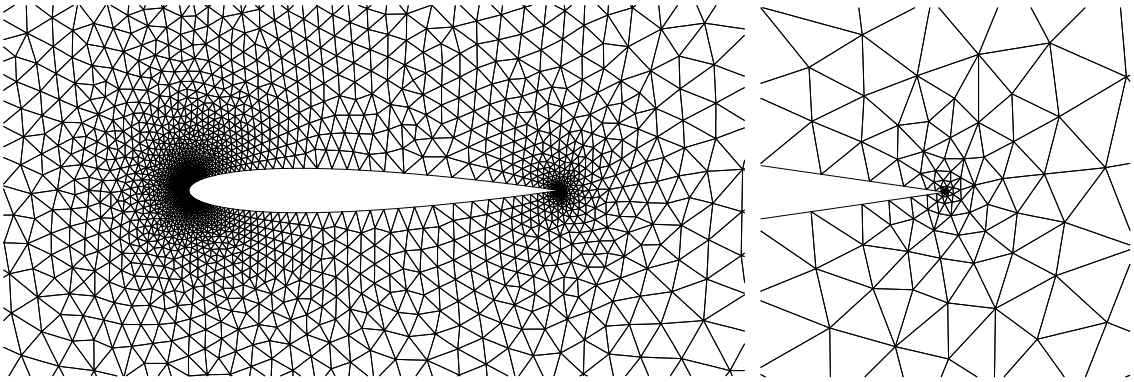

(a) $p = 1$, $\text{dof} = 20,000$, $\mathcal{E}_{c_d} = 2.9 \times 10^{-5}$

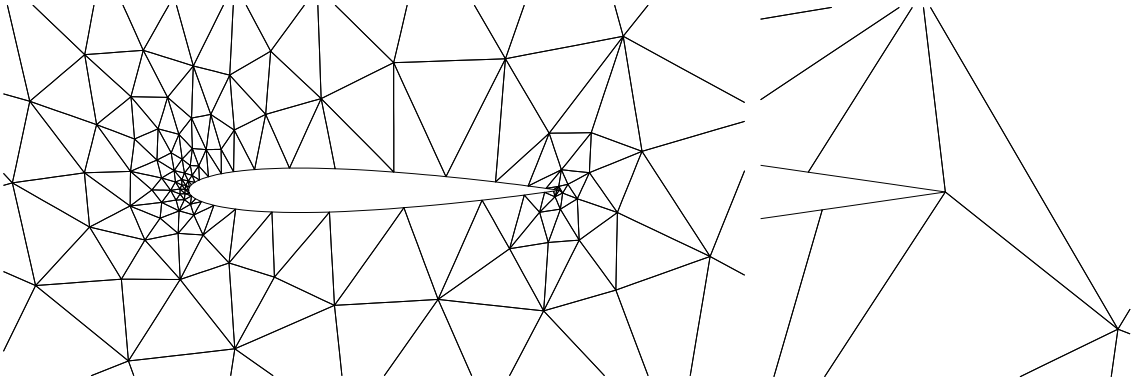

(b) $p = 3$, $\text{dof} = 5,000$, $\mathcal{E}_{c_d} = 2.8 \times 10^{-5}$

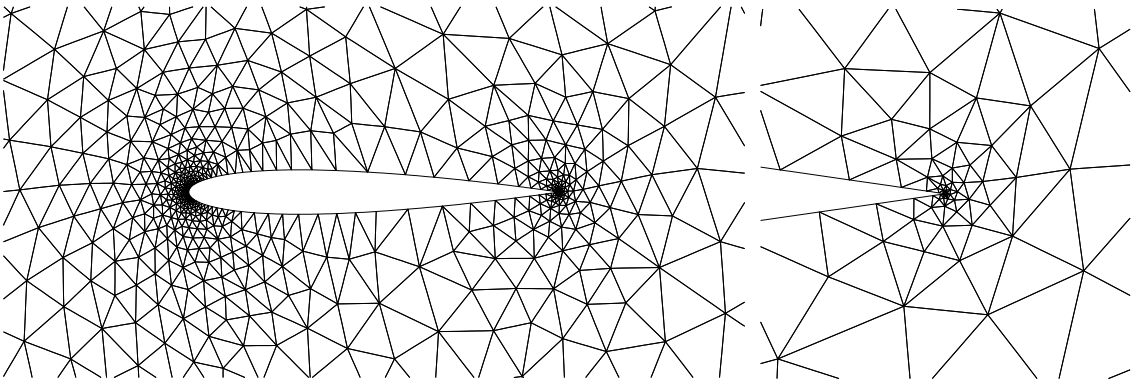

(c) $p = 3$, $\text{dof} = 20,000$, $\mathcal{E}_{c_d} = 2.9 \times 10^{-8}$

Figure 4. Select adapted meshes for the subsonic inviscid problem. Overview (left) and trailing edge zoom in the region $[c - \delta, c + \delta] \times [-\delta, \delta]$ with $\delta = 10^{-2}c$ (right).

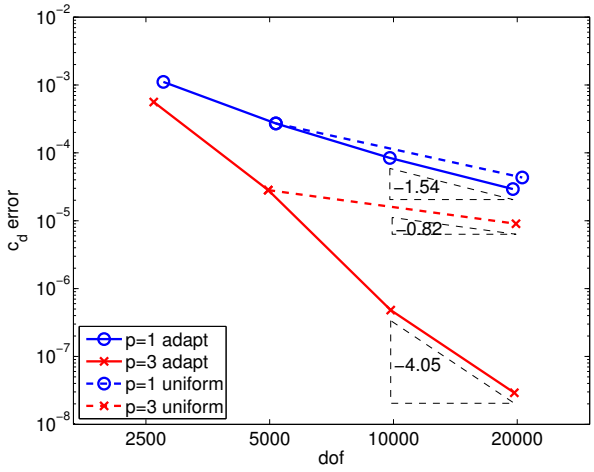

Figure 5. Comparison of adaptive refinement and a step of uniform refinement starting from adapted meshes for the subsonic inviscid case.

IV. Results: Transonic Inviscid ($M_\infty = 0.8$, $\alpha = 1.25°$)

IV.A. Error Convergence

The reference solution is obtained using the adaptive $p = 2$, dof $= 160000$ discretization. The reference c_d and c_l values used for this case are

$$c_d = 0.022628 \pm 1 \times 10^{-6}$$
$$c_l = 0.35169.$$

The error estimate for c_d is based on the adjoint-based error estimate and the fluctuation in the c_d value for this family of optimized meshes. We caution that the c_l reference value is likely less accurate than the drag value due to the ill-behaved lift output with the weakly enforced Kutta condition.

Figure 6 summarizes the convergence of the drag and lift coefficients against the number of degrees of freedom and the work unit. Despite the use of strongly graded anisotropic meshes as will be seen in Section IV.B, the $p = 2$ discretization is not more efficient than the $p = 1$ discretization in terms both the degrees of freedom and work unit. Furthermore, note that work unit for a given p-dof combination is substantially higher than in the subsonic inviscid case: for the $p = 2$, dof $= 20,000$ combination, 87 work units are required compared to the 15 work units for the subsonic case. The increase in the work unit is not only due to the more expensive residual evaluation with the addition of the viscous term and the shock PDE, but also due to a poorer convergence of the nonlinear solver in the presence of the shock.

IV.B. Comparison of Adapted Meshes

Drag-adapted meshes for the transonic inviscid flow at select p-dof combinations are shown in Figure 7. The flow exhibits a number of additional features that are absent in the subsonic condition, including: the shocks on the upper and lower surfaces; the primal solution discontinuity across the stagnation streamline downstream of the trailing edge; the dual solution discontinuity across the stagnation streamline upstream of the leading edge; and the adjoint discontinuity emanating from the root of the shock that reflects off the sonic line. Note that highly anisotropic elements are employed to resolve the directional features (e.g. shocks).

Comparison of the $p = 1$, dof $= 10,000$ mesh (Figure 7(a)) and the $p = 2$, dof $= 10,000$ mesh (Figure 7(b)) reveals the diffeences in the meshes required to achieve the drag error level of approximately 2×10^{-4} using the $p = 1$ and $p = 2$ discretizations. At this error level, the $p = 2$ adaptation focuses on resolving the shock and the discontinuity emanating from the trailing edge; the mesh is very sparse outside of these regions. The $p = 1$ discretization employs more elements to resolve the feature near the leading edge and the stagnation streamline.

Comparison of the $p = 2$, dof $= 10,000$ mesh (Figure 7(c)) and the $p = 2$, dof $= 40,000$ mesh shows how the mesh evolves for a given p to achieve a lower error level. With the addition of the degrees of freedom,

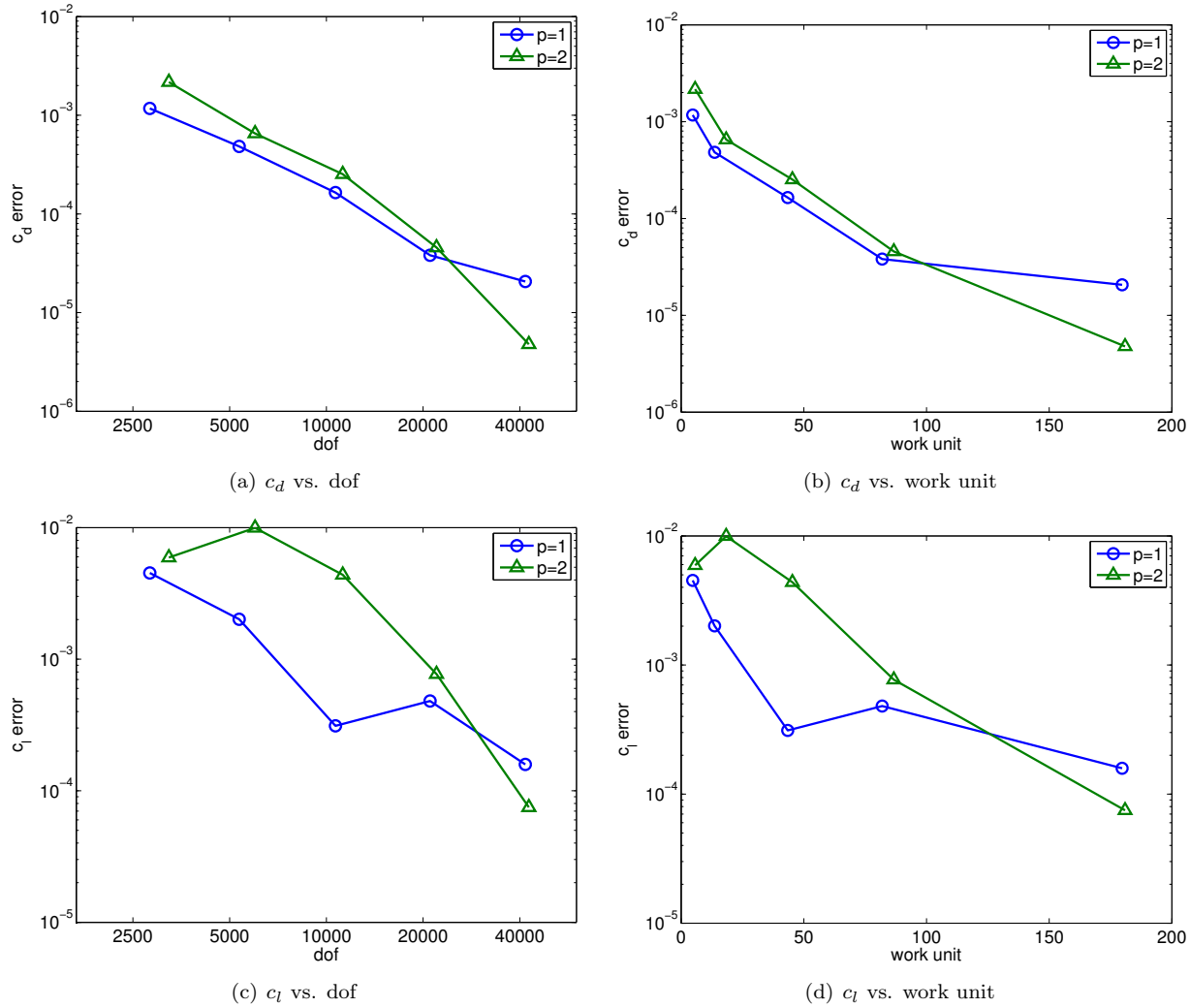

(a) c_d vs. dof

(b) c_d vs. work unit

(c) c_l vs. dof

(d) c_l vs. work unit

Figure 6. Error convergence for the transonic inviscid case.

the adaptation algorithm reveals and resolves more primal and adjoint features. The refinement towards the shock on the upper surface is also stronger than what would have been achieved by uniform refinement; the shock-normal length of the anisotropic elements decrease from $h_\perp \approx 3 \times 10^{-3} c$ at dof $= 10,000$ to $h_\perp \approx 1 \times 10^{-4} c$ at dof $= 40,000$, i.e. refinement by a factor of 30 as oppose to a factor of two. However, despite these solution-specific refinements, the adaptive algorithm is incapable of realizing the benefit of higher-order discretization for this shock-dominated case.

V. Results: Subsonic Laminar ($M_\infty = 0.5$, $\alpha = 1°$, $Re_c = 5,000$, $Pr = 0.72$)

V.A. Error Convergence

The reference solution is obtained using the adaptive $p = 3$, dof $= 80000$ discretization. The reference c_d and c_l values used for this case are

$$c_d = 0.0553167 \pm 3 \times 10^{-9}$$
$$c_l = 0.018274$$

The error estimates are based on the adjoint-based error estimates and the fluctuation in the output values for this family of optimized meshes.

Figure 8(a) shows the convergence of the drag coefficient against the number of degrees of freedom. With the proper mesh refinement, we recover the optimal output-error convergence rate of $h^{2p} = (\text{dof})^{-p}$

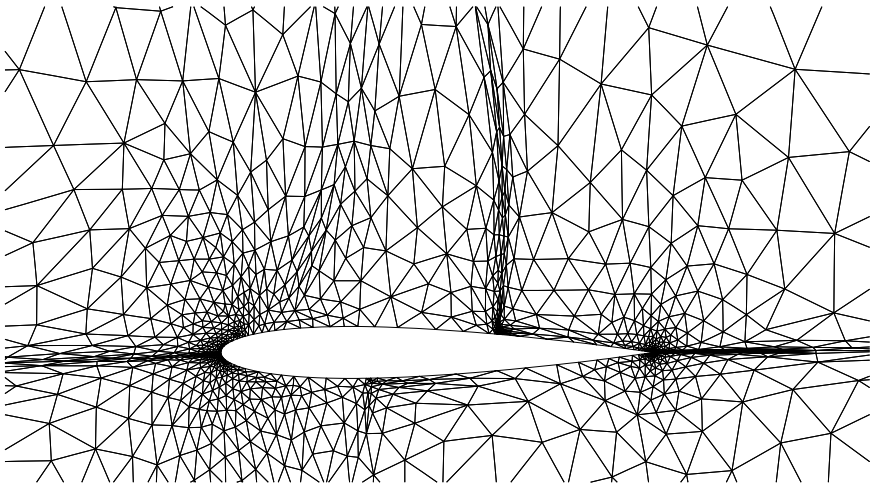

(a) $p = 1$, dof $= 10,000$, $\mathcal{E}_{c_d} = 1.6 \times 10^{-4}$

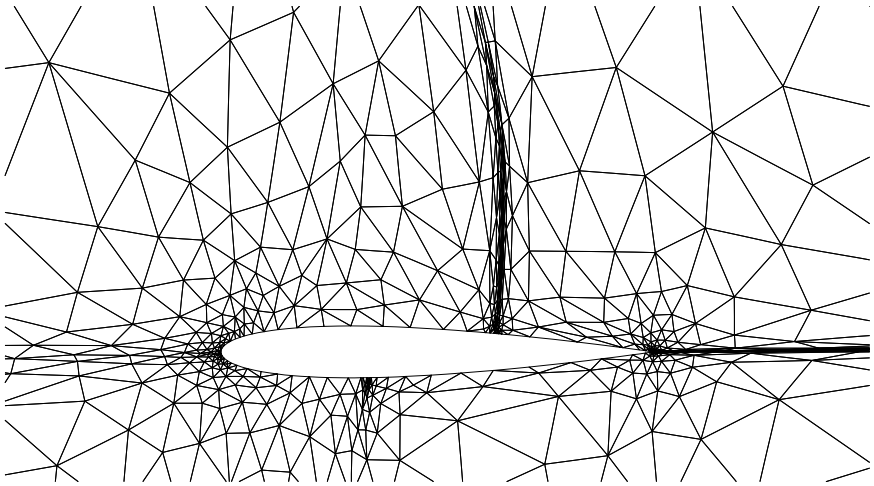

(b) $p = 2$, dof $= 10,000$, $\mathcal{E}_{c_d} = 2.5 \times 10^{-4}$

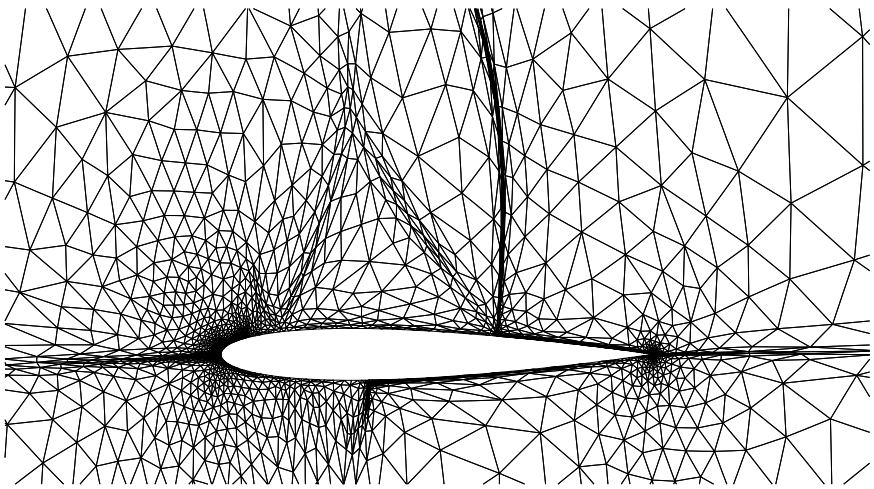

(c) $p = 2$, dof $= 40,000$, $\mathcal{E}_{c_d} = 4.8 \times 10^{-6}$

Figure 7. Select adapted meshes for the transonic inviscid problem.

for the viscous problem. (Note that the optimal output convergence rate for an viscous problem is h^{2p} for dual-consistent discretizations.) With uniform refinement, the convergence rate would be limited by the trailing edge singularity; in particular, the boundary layer, which is smooth, is not the feature that would limit the higher-order convergence. Similar to the inviscid case, the observed convergence rates are slightly higher than those predicted by the theory. The adaptive refinement allows the higher-order discretizations to achieve the near asymptotic performance using a small number of elements, making the $p > 1$ discretizations competitive for as high as 1 drag count of error. For a simulation requiring a tighter error tolerance, the higher order discretizations are clearly superior. Figure 8(b) shows that the $p > 1$ discretizations are more efficient than the $p = 1$ discretization also in terms of the work unit.

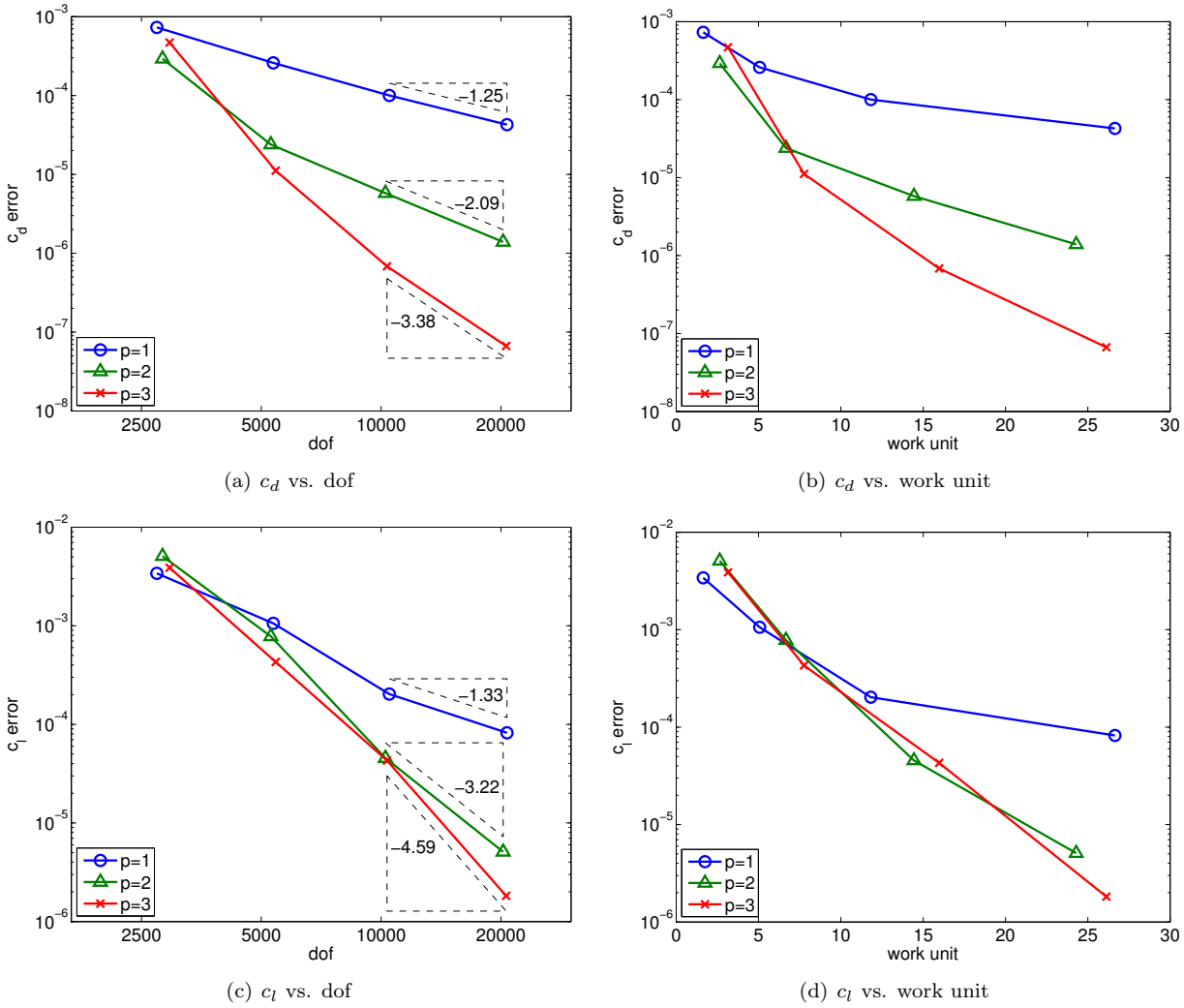

(a) c_d vs. dof

(b) c_d vs. work unit

(c) c_l vs. dof

(d) c_l vs. work unit

Figure 8. Error convergence for the subsonic laminar case.

The lift convergence result in Figure 8(c) shows that the $p > 1$ discretizations are more efficient than the $p = 1$ discretization except on the coarsest meshes. The less stable behavior of the lift output compared to the drag output may be partially due to the use of drag-adapted meshes. Our experience suggests that a stronger refinement along the stagnation streamline is necessary for an accurate lift calculation than drag calculation. We note that the output-based adaptation framework can be extended to generate a more flexible mesh that targets multiple outputs using, for example, the method of Hartmann.[12]

V.B. Comparison of Adapted Meshes

Drag adapted meshes for this subsonic laminar flow at select p-dof combinations are shown in Figure 9. The boundary layer is efficiently resolved using anisotropic elements; however, due to the relatively low Reynolds

number ($Re_c = 5000$), the aspect ratio of the elements is relatively low (compared to, say, a high Reynolds number RANS flow). We also note the presence of a singularity at the trailing edge for this case. Both the wake and stagnation streamline are refined to capture the directional features in the primal and dual solutions, respectively.

Comparison of the $p = 1$, dof $= 20,000$ mesh (Figure 9(a)) and the $p = 3$, dof $= 5,000$ mesh (Figure 9(b)) reveals the differences in the meshes required to achieve the drag error level of approximately 2×10^{-5} using the $p = 1$ and $p = 3$ discretizations. (Note that, though the $p = 3$ meshes uses four times fewer degrees of freedom, the $p = 3$ discretization is approximately four times smaller than the $p = 1$ discretization.) The $p = 3$ mesh is significantly sparser in the boundary layer region than the $p = 1$ mesh, as the boundary layer is a smooth feature that can be efficiently resolved using the higher-order approximation.

Comparison of the $p = 3$, dof $= 5,000$ mesh (Figure 9(b)) and the $p = 3$, dof $= 20,000$ (Figure 9(c)) mesh shows how the mesh evolves for a given p to achieve a lower error level. The refinement in the boundary layer region is mostly uniform. There is a strong refinement towards trailing edge singularity, which is the dominant singular feature of the flow.

VI. Conclusions

Using an output-based adaptive algorithm, subsonic inviscid, transonic inviscid, and subsonic laminar flows over a NACA 0012 airfoil were solved efficiently in a fully-automated manner starting from the same initial mesh. The benefit of the $p > 1$ discretizations were realized for the subsonic inviscid and laminar cases by controlling the effect of the trailing edge singularity via adaptive refinement. In particular, the higher-order discretizations achieved higher-efficiency even for the drag error level of as high as several drag counts. However, for the shock-dominated transonic inviscid case, the benefit of higher-order discretization could not be realized even with adaptation.

Acknowledgments

The authors would like to thank the entire ProjectX team for the many contributions that enabled this work. This work was supported by the Singapore-MIT Alliance Fellowship in Computational Engineering and The Boeing Company with technical monitor Dr. Mori Mani.

References

[1]P. L. Roe, Approximate Riemann solvers, parameter vectors, and difference schemes, J. Comput. Phys. 43 (2) (1981) 357–372.

[2]F. Bassi, S. Rebay, GMRES discontinuous Galerkin solution of the compressible Navier-Stokes equations, in: K. Cockburn, Shu (Eds.), Discontinuous Galerkin Methods: Theory, Computation and Applications, Springer, Berlin, 2000, pp. 197–208.

[3]G. E. Barter, D. L. Darmofal, Shock capturing with pde-based artificial viscosity for dgfem: Part i, formulation, J. Comput. Phys. 229 (5) (2010) 1810–1827.

[4]M. Yano, J. M. Modisette, D. Darmofal, The importance of mesh adaptation for higher-order discretizations of aerodynamic flows, AIAA 2011–3852 (Jun. 2011).

[5]Y. Saad, M. H. Schultz, GMRES: A generalized minimal residual algorithm for solving nonsymmetric linear systems, SIAM Journal on Scientific and Statistical Computing 7 (3) (1986) 856–869.

[6]L. T. Diosady, D. L. Darmofal, Preconditioning methods for discontinuous Galerkin solutions of the Navier-Stokes equations, J. Comput. Phys. 228 (2009) 3917–3935.

[7]P.-O. Persson, J. Peraire, Newton-GMRES preconditioning for discontinuous Galerkin discretizations of the Navier-Stokes equations, SIAM J. Sci. Comput. 30 (6) (2008) 2709–2722.

[8]M. Yano, D. Darmofal, An optimization framework for anisotropic simplex mesh adaptation: application to aerodynamic flows, AIAA 2012–0079 (Jan. 2012).

[9]R. Becker, R. Rannacher, An optimal control approach to a posteriori error estimation in finite element methods, in: A. Iserles (Ed.), Acta Numerica, Cambridge University Press, 2001.

[10]F. Hecht, Bamg: Bidimensional anisotropic mesh generator, `http://www-rocq1.inria.fr/gamma/cdrom/www/bamg/eng.htm` (1998).

[11]T. A. Oliver, A higher-order, adaptive, discontinuous Galerkin finite element method for the Reynolds-averaged Navier-Stokes equations, PhD thesis, Massachusetts Institute of Technology, Department of Aeronautics and Astronautics (Jun. 2008).

[12]R. Hartmann, Multitarget error estimation and adaptivity in aerodynamic flow simulations, SIAM J. Sci. Comput. 31 (1) (2008) 708–731.

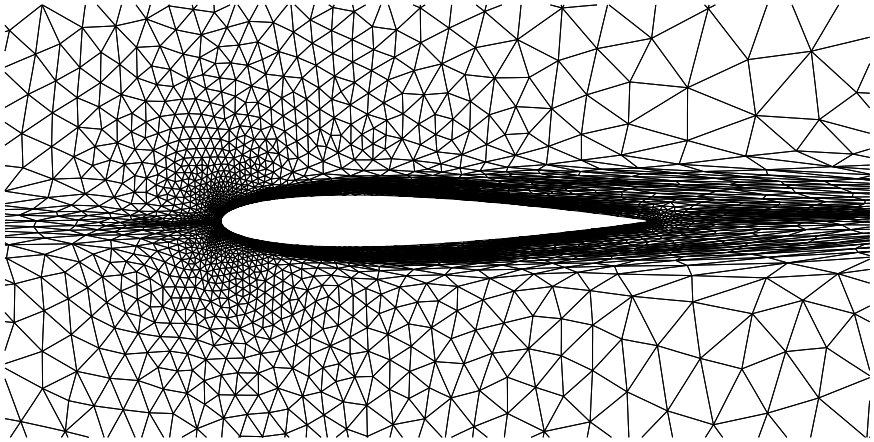

(a) $p = 1$, dof $= 20,000$, $\mathcal{E}_{c_d} = 4.3 \times 10^{-5}$

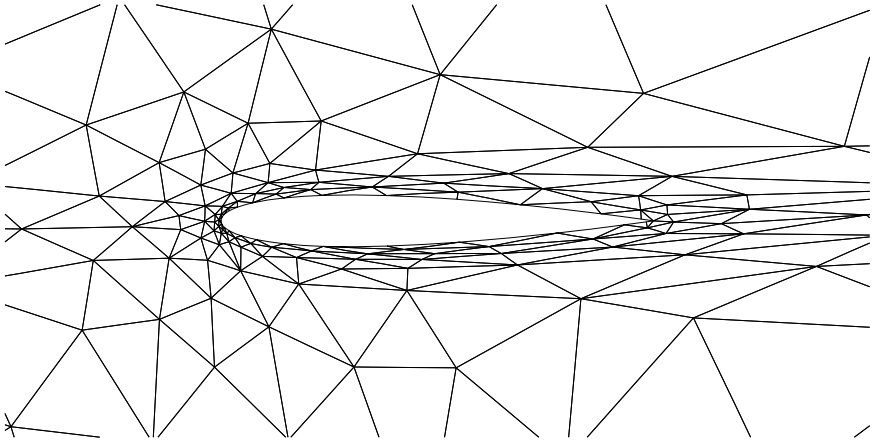

(b) $p = 3$, dof $= 5,000$, $\mathcal{E}_{c_d} = 1.1 \times 10^{-5}$

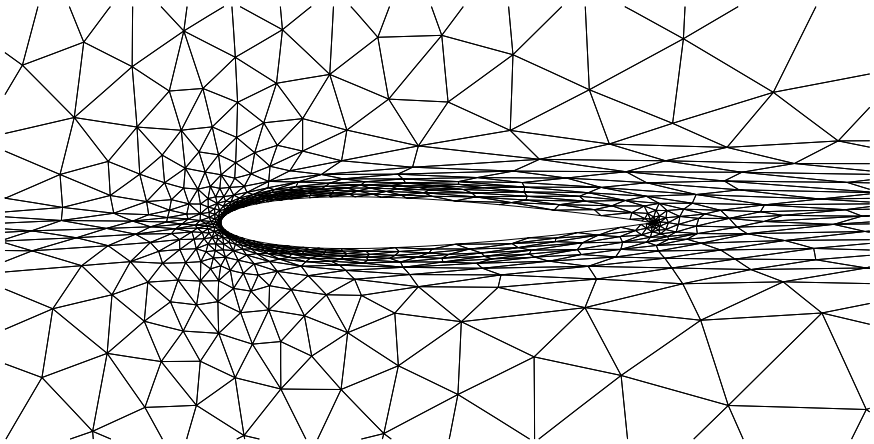

(c) $p = 3$, dof $= 20,000$, $\mathcal{E}_{c_d} = 6.7 \times 10^{-8}$

Figure 9. Select adapted meshes for the subsonic laminar problem.